International Conference on Ships and Offshore Structures
ICSOS 2016
31 August – 2 September 2016, Hamburg, Germany

Effect of Cutout on the Ultimate Strength of a Wind Turbine Tower

Sang Eui Lee[a], Selcuk Sahin[b,c], Philippe Rigo[b], Minsue Park[d], Jeom Kee Paik[a,d,e,*]

[a]*The Korea Ship and Offshore Research Institute (The Lloyd's Register Foundation Research Centre of Excellence), Pusan National University, Busan 46241, Republic of Korea*
[b]*Naval Architecture and Transport Systems Department (LHCN), University of Liège, 6 Quai Banning, B4000 Liège, Belgium*
[c]*Laboratoire d'Hydrodynamique, Energétique et Environement Atmosphérique (LHEEA), Ecole Centrale de Nantes, 44321 Nantes, France*
[d]*Department of Naval Architecture and Ocean Engineering, Pusan National University, Busan 46241, Republic of Korea*
[e]*Department of Mechanical Engineering, University College London, Torrington Place, London WC1E 7JE, UK*

Abstract

In wind turbine structures, cutouts are often located to make a way of access or passage. These perforations will reduce the ultimate strength of a wind turbine tower. The cutouts may thus need to be included in the ultimate strength formulations as a parameter of influence where significant. The aims of this study are to examine the effect of cutout on the ultimate-strength characteristics of the wind turbine tower, and to propose some practical design formulae to predict the ultimate strength. The structural features of the cutout and the tower in real wind turbines are investigated. The effect of different design variables, such as shape, location, aspect ratio, column slenderness ratio and column aspect ratio on the ultimate-strength behavior is described. The tower ultimate strengths are computed by elastic-plastic large-deflection finite element analyses. Thus, practical design formulae accommodating whole range of actual dimensional characteristics of the cutout and the tower have been derived and proposed. The findings of the research and the proposed design formulae have the potential to enhance the structural design and safety assessment of the wind turbine tower.

Keywords: Cutout; ultimate strength; wind turbine tower; parameters of influence; nonlinear finite element method.

1. Introduction

In steel-plated structures, cutouts are widely used to provide a way of access or to lighten the structure. It is no wonder that these perforations will reduce not only the buckling strength of structures but also the ultimate strength. In particular, a wind turbine which has relatively large size of a door will be exposed to considerable strength reduction that can potentially cause significant structural failure in the wind turbine tower. It is thus of great importance to develop advanced technologies which can predict the reduced strength of the tower by the size of the cutout.

The regulations for a reliable design and safety of wind turbines have been developed and recommended by various authorities (ECCS 1980, DIN 18800-4 1990, EN1993-1.6 2006, DNVGL 2013a and DNVGL 2013b). However, no detailed guidelines for predicting the reduced strength of towers are available.

It is noted that useful research attempts to investigate the effect of cutout on structural capacity of the wind turbine tower are relatively far less than plates (Sabir and Chow 1983, Brown and Yettram 1986, Azizian and Roberts 1983, Shangmugam et al. 1999, Durban and Zuckerman 1999, Betten and Shin 2000, El-Sawy et al. 2004, Paik 2007, Kim et al. 2009 and Wang et al. 2009). For a couple of decades, there were a number of researches related to buckling analysis of circular cylindrical shells(Brazier 1927, Reissner 1961, Seide and Weingarten 1961, Fabian 1977 and Gellin 1980) with the cutout under axial compression (Schenk and Schuëller 2007, Shariati and Rokhi 2010 and Ghazijahani

* Corresponding author. Tel.: +82-51-510-2429; fax: +82-51-518-7687.
E-mail address: jeompaik@pusan.ac.kr

Nomenclature

A	Area of the cutout	b	Breadth of the cutout
D (D_{max} / D_{min})	Diameter (maximum/minimum) of the wind turbine tower		
E	Elastic modulus of the material	F_R	Reference force of the wind turbine tower
F_{Tower}	Force acting on the wind turbine tower	F_u	Ultimate force of the wind turbine tower
F_{wind}	Thrust induced by blades	F_z	Load in z-axis
h	Height of the cutout		
h_o	Distance from the lower end to the centre of the cutout		
H	Height of the wind turbine tower	H_S	Height of 1st section
M	Pure bending moment	M_u	Ultimate bending moment
M_P	Plastic bending moment	M_y	Pure bending moment in y-axis
r	Radius	R	Corner radius of the cutout
R^2	Adjusted R-square		
t (t_{max} / t_{min})	Thickness (maximum/minimum) of the wind turbine tower		
t_c	Thickness of the cutout	T	Torque moment
u_x, u_y, u_z	Translational restraints in the x-, y- and z-axis		
w_o	Initial imperfection	W	Weight
α	Aspect ratio (height to breadth) of the cutout		
β	Slenderness ratio (breadth to thickness) of the cutout		
δ_{max}	Maximum deformation		
γ	Column aspect ratio (height to diameter) of the wind turbine tower		
γ_{max} / γ_{min}	Maximum/minimum column aspect ratio (height to maximum/minimum diameter) of the wind turbine tower		
λ	Column slenderness ratio (diameter to thickness) of the wind turbine tower		
λ_{max} / λ_{min}	Maximum/minimum column slenderness ratio (maximum/minimum diameter to maximum/minimum thickness) of the wind turbine tower		
ν	Poisson's ratio		
θ	Angle of the cutout in the circumferential direction		
$\theta_x, \theta_y, \theta_z$	Rotational restraint in the x-, y- and z-axis		
σ	Coefficient of correlation	σ_Y	Yield stress of the material
$\xi_D, \xi_t, \xi_h, \xi_b, \xi_C$	Coefficients of design formula for axial compression		
$\zeta_D, \zeta_t, \zeta_h, \zeta_b, \zeta_C$	Coefficients of design formula for pure bending		

et al. 2015) and pure bending (Yeh et al. 1999, Dimopoulos and Gantes 2012, 2013, 2015 Guo et al. 2013 and Dimopoulos et al. 2015).

The aims of this study are to use nonlinear finite element analysis to examine the effect of cutout on ultimate-strength characteristics and to propose simple design formula to estimate the reduced ultimate strength of the wind turbine tower under axial compression and pure bending. The structural features of wind turbines are investigated using data collected from 102 existing wind turbines in service. Finite element modelling techniques are developed to calculate the ultimate-strength behavior of the tower with a variety of design variables, such as cutout's shape and location, aspect ratio, column slenderness ratio and column aspect ratio. The validation of developed nonlinear finite element method modelling is conducted. For parametric series analyses, design of experiment (DOE) method such as central composite design (CCD) is applied. Numerical computations are used to derive a plausible design formula that predicts the ultimate strength of the tower.

2. Literature Review

In the early days, the buckling analysis of circular cylindrical shells analytically and experimentally involved. In particular, Brazier (1927) noted that the ultimate strength is directly related to the ovalization of the tube cross-section under bending and derived an expression for the strain energy per unit tube length in terms of the change in axial curvature. Reissner (1961) further developed the more general formulation for thin-walled cylindrical shells of arbitrary cross section. By using a modified Donnell equation and the Galerkin method, Seide and Weingarten (1961) found out that the maximum elastic bending buckling stress is equal to the critical compressive stress under axial compression. Sherman (1976) experimentally identified that shells with column slenderness ratio, greater than

about 50 do not have sufficient plastic hinge rotation capacity to develop the classical ultimate strength. Fabian (1977) observed two modes of failure of infinitely long cylindrical elastic shells subjected to bending, pressure and axial loads; the circumferential flattening constituting an ultimate load and compression wrinkles generating bifurcation buckling axially. Gellin (1980) demonstrated the example of extending the results of Brazier (1927) into the plastic range and confirmed the results of limit states observed by Fabian (1977).

Traditionally, experimental tests have been regarded as the most efficient way of obtaining technical solutions despite its high costs. Over the past 50 years, computing speeds and capabilities of numerical tools have been significantly enhanced. Hence, a contribution of numerical simulations to the engineering applications is higher than before. The same trend observed in wind turbine industries and a number of experiment tests and numerical simulations have been extensively carried out to examine the load carrying capacity of circular cylindrical shells with a cutout under axial compression and pure bending.

For axial compression, Tennyson (1968) experimentally observed a membrane stress distribution and isoclinic patterns around the edge of the cutout by using photo-elastic shells. Jullien and Limamto (1998) found that the buckling strength is sensitive to the cutout angle or circumferential size based on parametric studies of the shape (square, rectangular, circular), the dimensions (axial and circumferential sizes, diameter) of the cutout, furthermore, he pointed out the importance of initial imperfections for numerical simulations. Schenk and Schuëller (2007) studied the effect of random geometric imperfections on the critical load of thin-walled cylindrical shells under axial compression with rectangular cutouts and found that the coefficient of variation of the critical load does not decrease with decreasing the imperfections magnitude. Han et al. (2006) observed that the location and the size of the cutout significantly affect the buckling load. Namely, cutouts located near the loaded end could effectively absorb energy, and redistribute the load more efficiently. Shariati and Rokhi (2008, 2010), reported that longer shells show much more sensitive to the position of the cutout. Moreover, they observed that the buckling strength decreases as height increases with the constant cutout width. Ghanbari Ghazijahani et al. (2015) experimentally found a symmetric ring-shaped bulging wave in the intact specimen after initiation of the buckling. It was observed that the effect of the cutout height on the capacity reveals less than 5% under axial compression.

For pure bending, Kyriakides and Ju (1992) and Ju and Kyriakides (1992) observed that thinner shells develop short wavelength periodic ripples on the compressed side of the shell, and the shells buckled locally and collapsed soon after the appearance of the ripples. On the other hand, thicker shells were found to exhibit limit load instability as a direct consequence of the ovalization of the shell cross-section caused by pure bending. Yeh et al. (1999) observed that for a shell with the circular

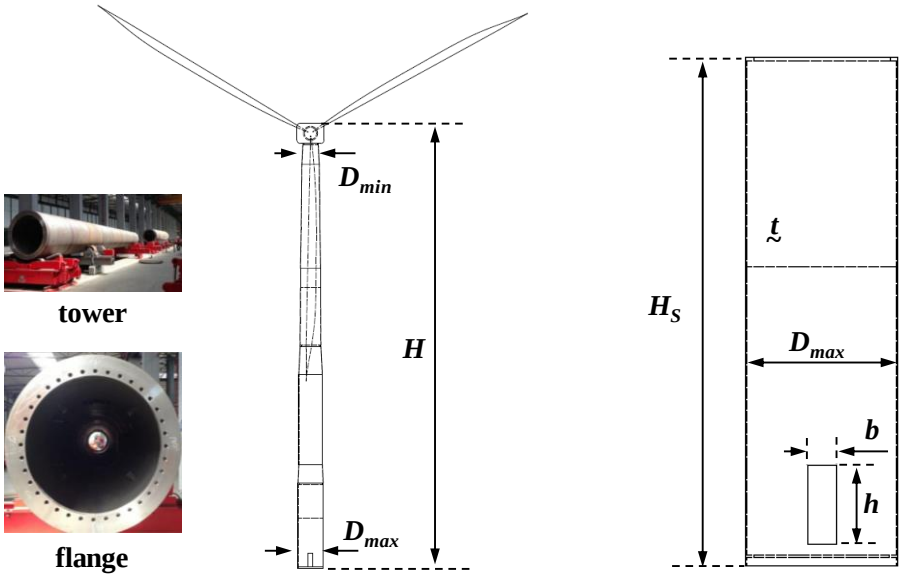

Fig. 1. An example of the wind turbine tower with the cutout.

cutout, the ultimate strength is decreased as the diameter of the cutout increases; for a shell with a rectangular cutout, the ultimate strength is decreased on increasing the size of the cutout. It was also found that the ultimate strength of a shell with the cutout on compression side is smaller than for the cutout on the tension side and the ultimate strength increased when the cutout is close to the end of the clamped shell. Guo et al. (2013) found that with the increase of D/t ratio, the local buckling phenomenon became more pronounced and the stiffeners increased the load carrying capacity and improved the ductility as well.

The most distinguished numerical and experimental works are Dimopoulous′s series of studies (Dimopoulos and Gantes 2012, Dimopoulos and Gantes 2013, Dimopoulos and Gantes 2015 and Dimopoulos et al. 2015) for circular cylindrical shell structures. Through experimental and numerical studies of the buckling behavior for cantilevered circular cylindrical shells with the cutout and stiffening were conducted. It was confirmed that the presence of the cutout leads to a strength reduction and the lowest collapse load appears when the cutout is situated on the compression side (Dimopoulos and Gantes 2012). Furthermore, it was found that simple stiffening types consisting of either a peripheral frame or two longitudinal stiffeners with a ring are particularly efficient and can be used instead of more complex ones (Dimopoulos and Gantes 2013). It was pointed out that the importance of geometrical and material nonlinearities including initial imperfections (Dimopoulos and Gantes 2015). At last, an assessment of stiffening effect of the cutout on circular cylindrical shells under dynamic wind loading was conducted by using aero-elastic code. It was concluded that the dynamic effect leads to a small decrease of tower strength compared to the one obtained via static analysis, but this reduction was less than 10% in all investigated cases (Dimopoulos et al. 2015).

3. Structural Features of the Wind Turbine Tower and the Cutout

3.1. Definition of geometrical parameters

Wind turbines typically consist of some of circular cylindrical shell sections which are connected with each other by bolted flanges as shown in Fig. 1. The geometrical attributes of a typical wind turbine tower with the cutout are defined. The following four parameters for wind turbine towers are considered: (a) minimum column aspect ratio ($\gamma_{min} = H / D_{min}$); (b) maximum column aspect ratio ($\gamma_{max} = H / D_{max}$); (c) minimum column slenderness ratio ($\lambda_{min} = D_{min} / t_{min}$); (d) maximum column slenderness ratio ($\lambda_{max} = D_{max} / t_{max}$). The other two parameters for the cutout are considered: (e) aspect ratio ($\alpha = h / b$); (f) slenderness ratio ($\beta = b / t_c$).

3.2. Geometrical features

Data on 102 wind turbines and their cutouts are collected where the capacity range from 0.5 to 5.0 MW. The principal features are displayed in Appendix, Table A1. The geometrical characteristics of each parameter predefined in Section 3.1 are then analyzed. The statistical distribution of the parameter is shown in Figs. 2 and 3. Table 1 summarizes the range and most probable values of each parameter. These findings are used to identify the geometrical parameters of the standard wind turbine tower and the cutout, as follows: H = 65,000 mm, $D_{\max}$ = 3,750 mm, t_{max} = 30 mm, h = 1,900 mm, b = 700 mm and t_c = 30 mm (α = 2.875, β = 25.0). It was assumed that the standard wind turbine tower is composed of four sections as shown in Fig. 4 and the height of 1st section which is used in the present

Table 1. Actual range and the most probable dimensions of the wind turbine and the cutout

Parameter	Range	Most probable	Parameter	Range	Most probable
Capacity (MW)	0.5~5.0	2.5	$t_{\max}$ (mm)	16~40	30
H (mm)	37,000~100,000	65,000	γ_{min}	17.5~42.1	30.0
h (mm)	1,640~2,900	1,900	γ_{max}	12.0~27.7	19.0
b (mm)	620~1,100	700	λ_{min}	100.0~250.0	170.0
t_c (mm)	16~40	30.0	λ_{max}	95.7~222.2	110.0
$D_{\min}$ (mm)	1,600~3,000	2,300	α	2.2~3.8	2.875
$D_{\max}$ (mm)	2,610~6,000	3,750	β	19.1~43.8	25.0
$t_{\min}$ (mm)	10~20	15			

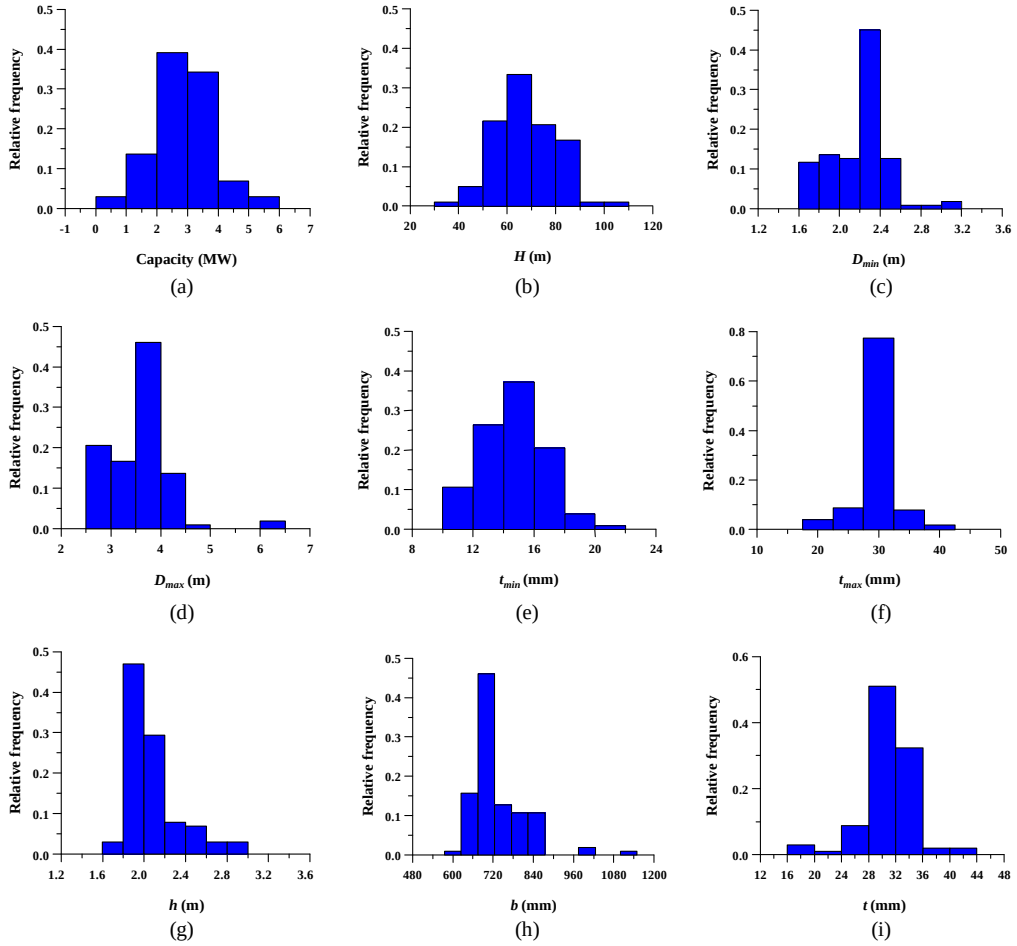

Fig. 2. Characteristics of the wind turbine tower and the cutout: (a) capacity; (b) height; (c) maximum diameter; (d) minimum diameter; (e) minimum thickness; (f) maximum thickness; (g) height of the cutout; (h) width of the cutout; (i) thickness of the cutout.

study is H_S = 12,655 mm. Hereafter, the thickness of the cutout, t_c and the maximum thickness of the wind turbine tower, $t_{\max}$ will be represented as the thickness of the wind turbine tower, t ($=t_c=t_{\max}$).

3.3. Reference capacity of circular cylindrical shells without the cutout

In the section of wind turbine structures with the cutout, the first yield occurs near the cutout where the highest compression develops and rapidly expands around the cutout with the further loading. The entire load carrying capacity of the wind turbine structure with the cutout depends on the geometrical dimensions as well as material properties. In the present study, the reference buckling loads of the shell without the cutout subjected to axial compression (Shariati and Rokhi 2008) and pure bending moment (Dimopoulous and Gantes 2013) are defined to be:

$$F_R = \pi D_{\max} t \times \sigma_Y \tag{1}$$

$$M_P = \frac{4}{3}\pi\left(\left(r+\frac{t}{2}\right)^3-\left(r-\frac{t}{2}\right)^3\right)\times\sigma_Y \tag{2}$$

where F_R is the reference load of wind turbine, M_P is plastic bending moment of wind turbine, $D_{\max}$ is the diameter of the wind turbine tower, r is the radius of the wind turbine tower, t is the thickness of the wind turbine tower, and σ_Y is the yield stress of the material.

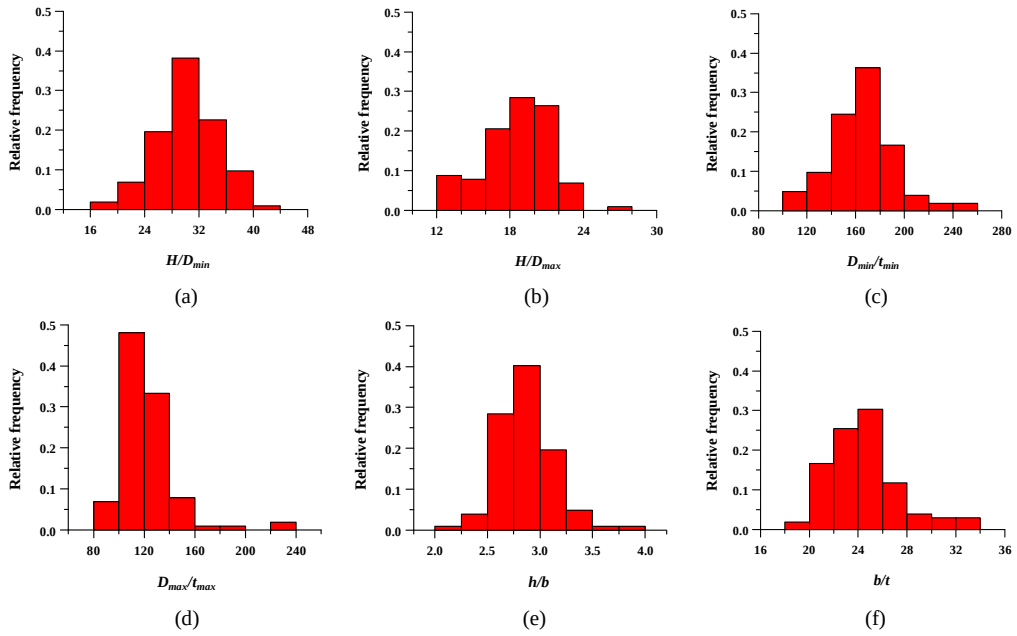

Fig. 3. Geometrical characteristics: (a) height to min. diameter ratio; (b) height to max. diameter ratio; (c) min. diameter to min. thickness ratio; (d) max. diameter to max. thickness ratio; (e) height to width ratio of the cutout; (f) width to thickness ratio of the cutout.

4. Nonlinear Finite Element Modelling

4.1. Finite element model

Nonlinear finite element analysis is performed using ANSYS-Workbench (2015), to accommodate both geometrical and material nonlinearities. The SHELL181 element, which has four nodes with six degrees of freedom at each node, is used to model circular cylinder shells and the SOLID185 element, which has eight nodes with three degrees of freedom at each node, is used to model the ring frame where located at both ends of the circular cylinder shell section. The wind turbine is modelled based on the result of quasi-static material test as shown in Fig. 5.

As noted by previous researches (Jullien and Limamto 1998, Schenk and Schuëller 2007 and Dimopoulos and Gantes 2015), the effect of initial imperfection is properly applied. The maximum magnitude of initial deflection w_o is assumed to be 30% of the thickness of the wind turbine tower; that is, $w_o = 0.3t$. The eigenvalue buckling mode is used to determine the shape of the initial deflection. Fig. 6 provides examples of the smallest buckling mode near the cutout obtained from the eigenvalue buckling analysis for intact (no opening) and with the cutout under axial compression and pure bending. For simplicity of finite element method computations, the residual stress caused by welding is not considered in the present study.

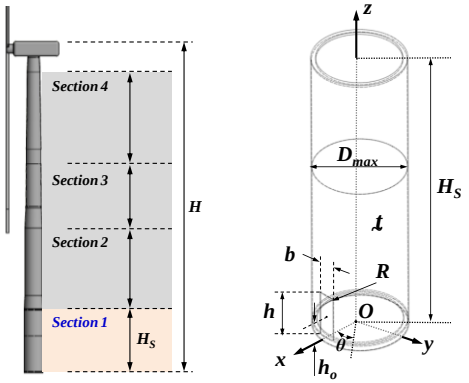

Fig. 4. Schematic representation of applied geometries.

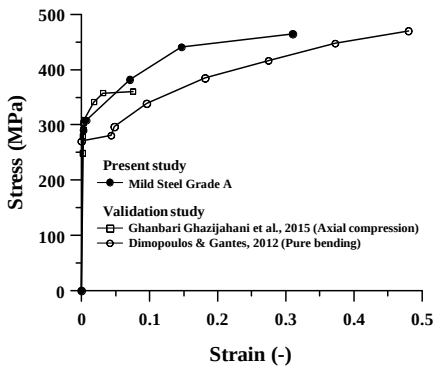

Fig. 5. Stress-strain curves for the applied materials.

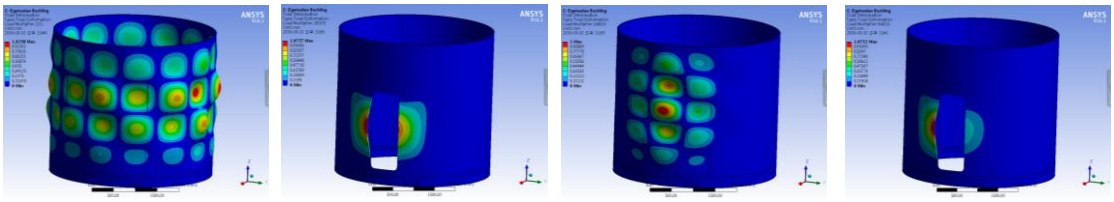

Fig. 6. An example of 1st buckling mode: (a) intact under axial compression; (b) with the cutout under axial compression; (c) intact under pure bending; (d) with the cutout under pure bending.

4.2. Loading conditions

The loading regimes of wind turbines during operations are extremely complex. A proper understanding of loads on wind turbines as well as the structural response is crucial to avoid their catastrophic failure. In general, the types of loads acting on wind turbines in service can be classified into five categories, static, cyclic, stochastic, aerodynamic and mechanical loads. As shown in Fig. 7, the schematic free-body diagram of a wind turbine structure would be represented as three loads; (a) a torque due to blades, (b) an axial force due to gravity, (b) a bending moment due to a thrust of blades and the transverse force on a tower.

In the present study, it is assumed that an axial force and bending moment are closely related to the wind turbine tower failure or collapse. To precisely investigate the effect of each load on the ultimate strength of the wind turbine tower with the cutout, it is applied as an isolated manner rather than in combination. However, it is essential to accurately predict the ultimate strength, the loads in combination should be taken into account.

4.3. Boundary conditions

The boundary conditions investigated in this study are described in Fig. 8. The coordinate system used for their measurement is shown in Fig. 8(a). The restraints are described in detail below.

- Fixed boundary condition, as shown in Fig. 8(b)
- Bottom surface: translational restraints in the *x*-, *y*- and *z*-directions, $u_x = u_y = u_z = 0$; rotational restraint in the *x*-, *y*- and *z*-direction, $\theta_x = \theta_y = \theta_z = 0$.

As mentioned earlier, a wind turbine with the cutout detailed in Section 3.2 is regarded as subjected to axial compression in z-axis and pure bending moment in y-axis as shown in Fig. 8(c).

4.4. Mesh-convergence study

This section presents the results of mesh-convergence study for 6-type of element sizes under pure bending when σ_Y = 299 MPa and $w_o = 0.3t$. In the mesh convergence study, six element sizes are tested under pure bending. The ultimate strength is summarized in Fig. 9. It is found that approximately 35,000 elements (F5, size= 40 mm) are sufficient to estimate the ultimate bending moment of the wind turbine. The authors assume that the mesh-convergence for axial compression may agree with the result of pure bending.

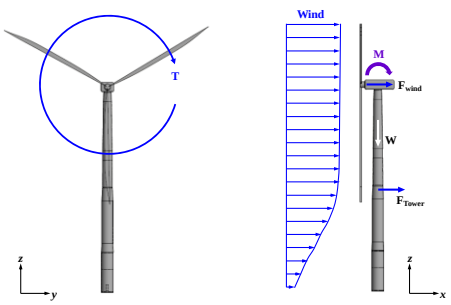

Fig. 7. Schematic free-body diagram.

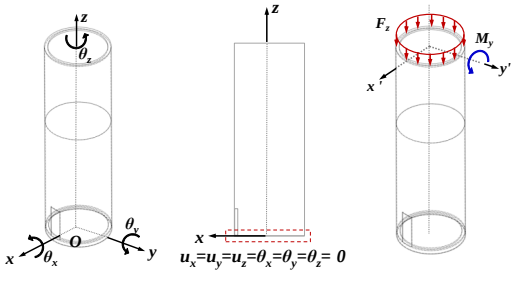

Fig. 8. Coordinate system and applied boundary conditions of the wind turbine tower: (a) coordinate system; (b) fixed boundary condition; (c) applied loading conditions.

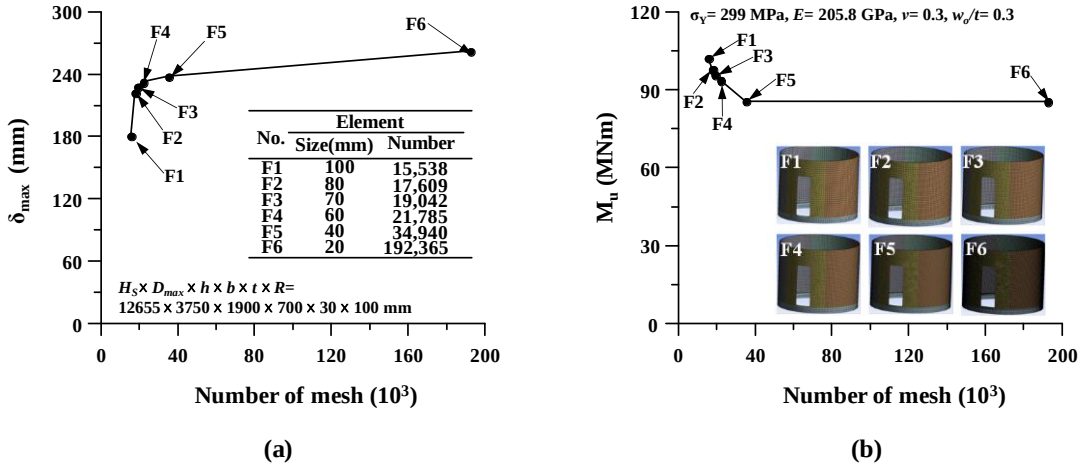

Fig. 9. Result of mesh-convergence: (a) maximum deformation; (b) maximum bending moment.

4.5. Validation

The finite element modelling techniques developed in the present study are validated with the experimental results under axial compression (Ghanbari Ghazijahani et al. 2015) and pure bending (Dimopoulos & Gantes 2012). Fig. 11 shows the results of validation study for the models as shown in Fig. 10. It was confirmed that the developed finite element modelling technique is effective for simulating the ultimate strength of the wind turbine tower under axial compression and pure bending.

5. Effect of Variables

In this section, three sets of parametric studies with the results are presented. First, to investigate the effects of cutout's shape on the ultimate strength, three shapes including rectangular, elliptical and half-elliptical-rectangular are considered. Second, to examine the effect of cutout's locations in vertical- and circumferential-direction on the ultimate strength, five locations in vertical direction and nine locations in circumferential direction are considered. Third, cutout's shape, aspect ratio, column slenderness (diameter to thickness) ratio and column aspect ratio (height to diameter) are taken as the design variables; their effects on the ultimate strength are widely calculated. To identify the combined effects of these variables on the ultimate strength, DOE with CCD method is applied for the selection of design points for a given range of each parameter from Section 3.2.

5.1. Effects of cutout's shape

As stated earlier, former researchers (Julien and Limam 1998, Yeh et al. 1999) attempted to examine the effect of cutout's shape on the load carrying capacity of the circular cylindrical shells. They concluded that existence of cutouts alters the nature of the moment-end-rotation response under pure bending. However, the effect of the cutout's shape on the load carrying capacity was weak and sometimes negligible.

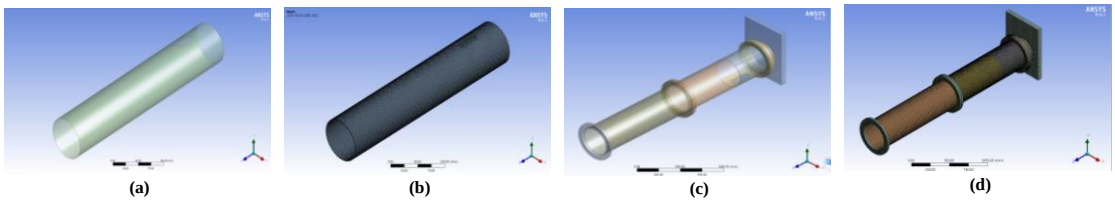

Fig. 10. Geometries and mesh models of validation studies: (a) geometry for axial compression; (b) applied mesh for axial compression; (c) geometry for pure bending; (b) applied mesh for pure bending.

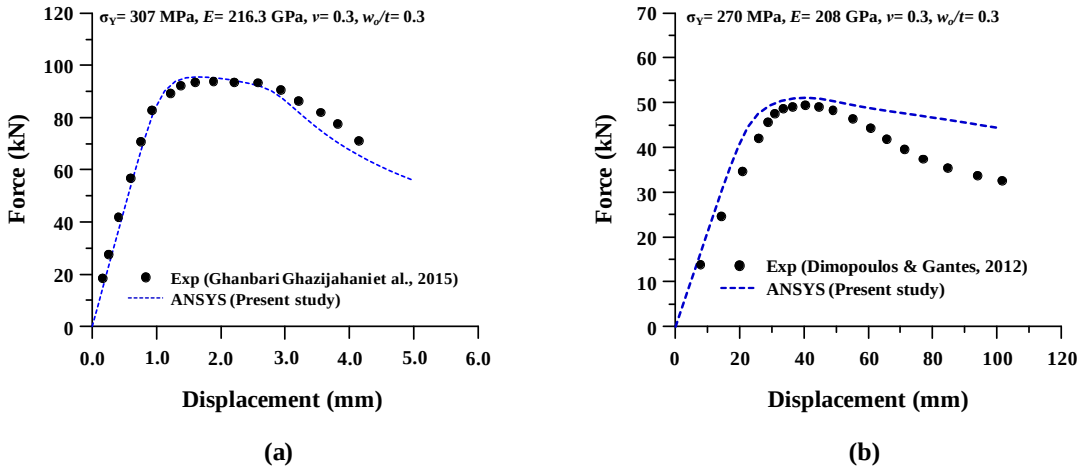

Fig. 11. Validation of developed finite element modelling technique; (a) axial compression; (b) pure bending.

The authors attempted to improve the understanding of the effects of the cutout's shape on the ultimate strength by using the standard model predefined in Section 3.2. Three-type of shapes including rectangular, elliptical, and half-rectangular-elliptical are considered. To perform accurate comparison, the area of the cutout, A was kept in the same. The parameters considered in this section are as follows:

- Shape: intact (no-opening), rectangular, elliptical, half-rectangular-elliptical
- Loading condition: axial compression, pure bending

Applied geometries are illustrated on Fig. 12 and their dimensions of the cutout are summarized in Table 2. Fig. 13 describes the comparison of the load carrying capacity against the no-opening model. It is found that the reduction rate of the ultimate strength of each shape for both loading conditions appears around 80% of intact. The present results confirm the previous findings (Julien and Limam 1998, Yeh et al. 1999) that the effect of shape is negligible.

5.2. Effects of cutout's location

The effect of cutout's location in vertical or circumferential directions was previously investigated by a number of researchers (Kyriakides and Ju 1992, Ju and Kyriakides 1992, Yeh et al. 1999, Han et al. 2006, Dimopoulos and Gantes 2012). It was noted that as the cutout's location closes to the loaded end, the ultimate strength increases under axial compression and the ultimate strength of a circular cylindrical shell with the cutout on compression side is smaller than that for the cutout on the tension side under pure bending (Kyriakides and Ju 1992, Ju and Kyriakides 1992, Yeh et al. 1999, Dimopoulos and Gantes 2012). To assess the ultimate strength of circular cylindrical shells with the cutout, a series of nonlinear finite element method computations are performed for various cutout's locations in vertical and circumferential directions.

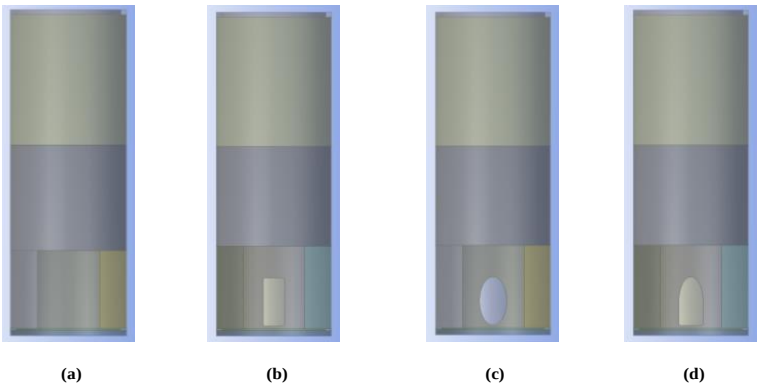

Fig. 12. An example of applied geometries: (a) intact (no opening); (b) rectangular; (c) elliptical; (d) half-rectangular-elliptical.

Table 2. Applied dimensions of cutout's shape

Shape	A ($\times 10^6$ mm^2)	h (mm)	b (mm)	R (mm)
Rectangular	1.321	1900	700.0	100
Elliptical	1.321	1900	885.5	-
Half-Rectangular-Elliptical	1.321	1900	781.6	100

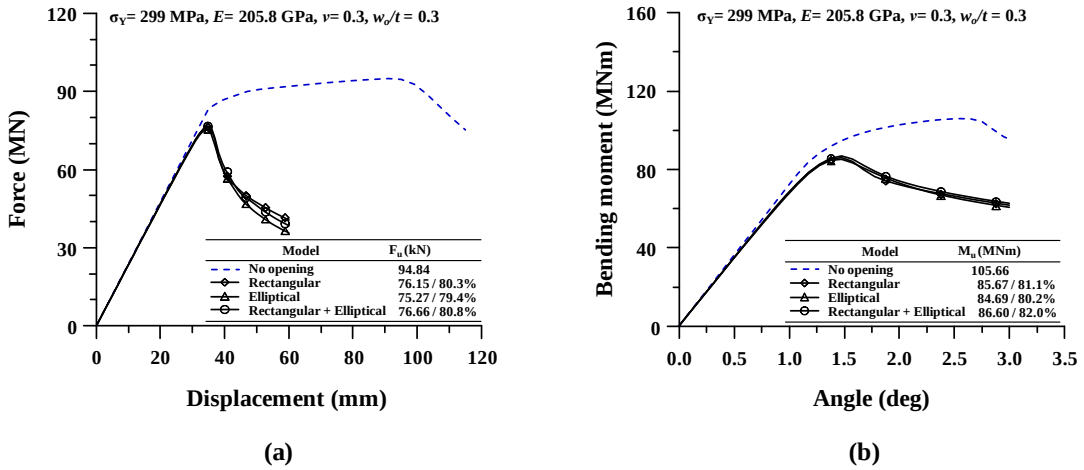

Fig. 13. Effect of cutout's shapes on load carrying capacity: (a) axial compression; (b) pure bending.

5.2.1. Vertical direction

In order to investigate the effect of cutout's location in vertical direction on the ultimate strength, the thickness, t is kept the same as 30 mm. Fifty cases of series analyses were performed in total. The parameters considered in this section are as follows:

- Shape: elliptical
- Location in vertical direction, h_o / H_S : 0.1, 0.2, 0.3, 0.4, 0.5
- Column slenderness ratio, $\lambda = D_{\max} / t$: 90, 110, 125, 130, 150
- Loading condition: axial compression, pure bending

Fig. 14 displays an example of applied geometries with varying cutout's location in vertical direction, $h_o / H_S = 0.1 \sim 0.5$. Figs. 15 and 16 illustrate the force-displacement and moment-rotation histories for various column slenderness ratios. It was found that as the cutout closes to the fixed boundary, the ultimate strength increases in both loading conditions. It indicates that the cutout located

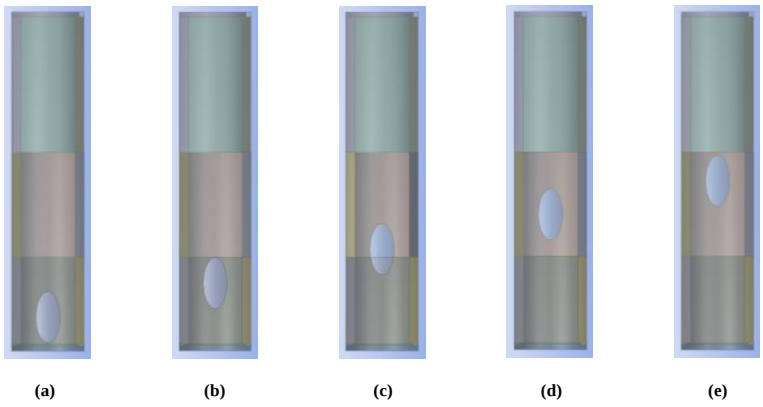

Fig. 14. An example of applied geometries with varying cutout's location in vertical direction: (a) $h_o / H_S = 0.1$; (b) $h_o / H_S = 0.2$; (c) $h_o / H_S = 0.3$; (d) $h_o / H_S = 0.4$; (e) $h_o / H_S = 0.5$.

near the loaded end could effectively absorb energy, and efficiently redistribute the load to the boundaries. It is observed that the ultimate strength under axial compression shows higher sensitivity than pure bending. Therefore, it is recommended that a structural design engineer should carefully consider the effect of cutout's location on the ultimate strength in axial compression. Fig. 17 summarizes the non-dimensionalized load carrying capacity varying cutout's location in vertical direction. It is observed that the ultimate strength increases almost linearly as a function of the cutout's location. It was found that as the column slenderness ratio decreases, the reduction rate increases in both loading conditions and the ultimate strength under pure bending is not sensitive to the variation of column slenderness ratio, namely, increasing diameter except for $\lambda = 150$.

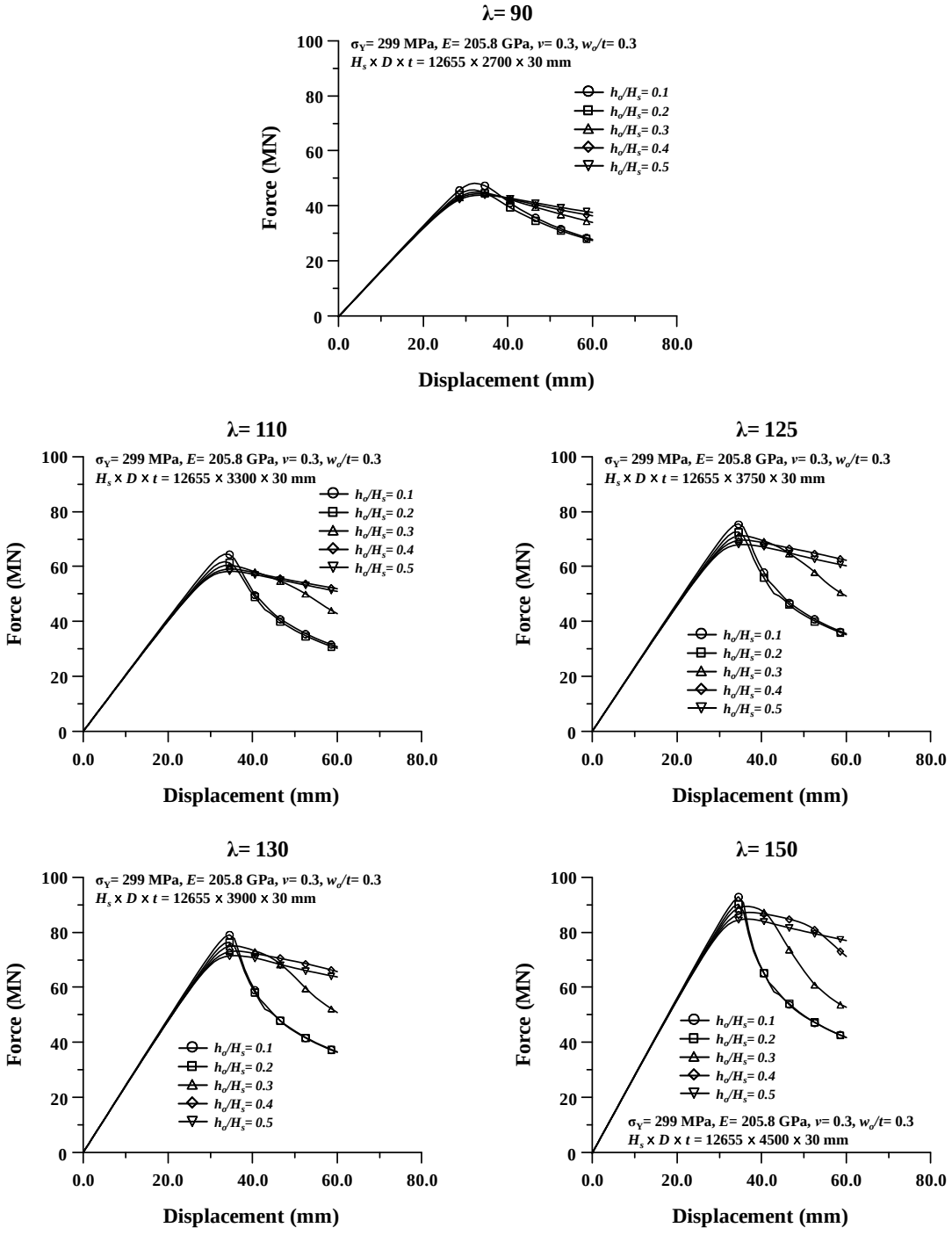

Fig. 15. Effect of cutout's location with varying column slenderness ratios under axial compression.

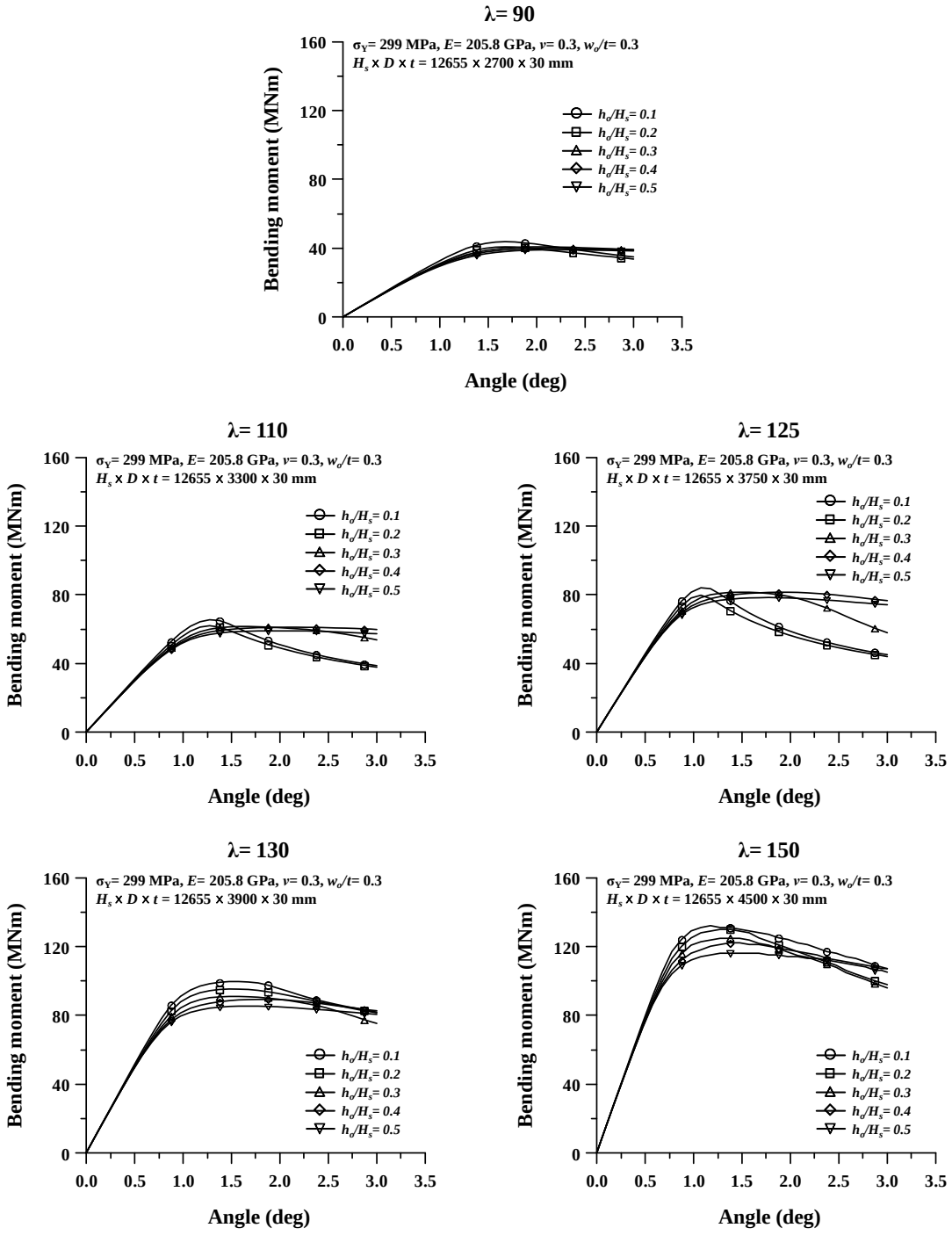

Fig. 16. Effect of cutout's location with varying column slenderness ratios under pure bending.

5.2.2. Circumferential direction

To identify the effect of cutout's location in circumferential direction on the ultimate strength, the thickness is kept the same as 30 mm for pure bending since the structural response under axial compression is symmetrical. Nine cases of series analyses are performed in total. The parameters considered in this section are as follows:

- Shape: half-rectangular-elliptical
- Cutout's angle, θ : 0, 15, 30, 45, 60, 90, 120, 150, 180 degree
- Loading condition: pure bending

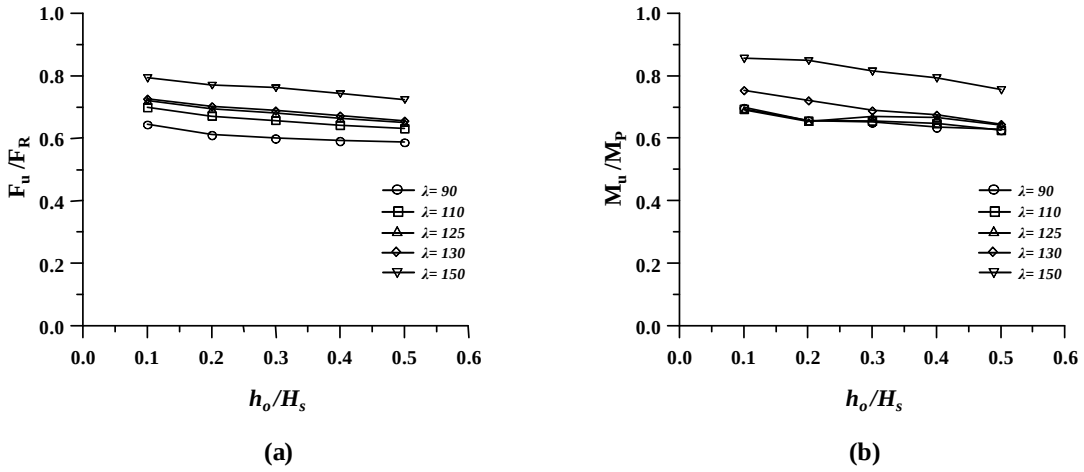

Fig. 17. Summary of non-dimensionalized load carrying capacity with varying cutout's location in vertical direction: (a) axial compression; (b) pure bending.

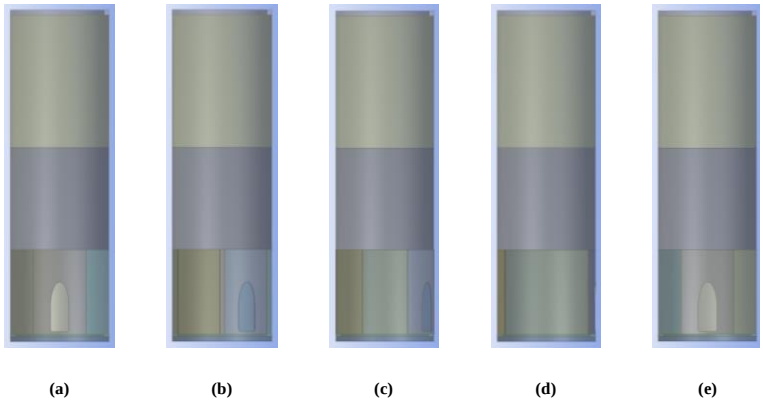

Figure 18. An example of applied geometries varying cutout's angle in circumferential direction: (a) $\theta = 0$ degree; (b) $\theta = 30$ degree; (c) $\theta = 60$ degree; (d) $\theta = 90$ degree; (e) $\theta = 180$ degree.

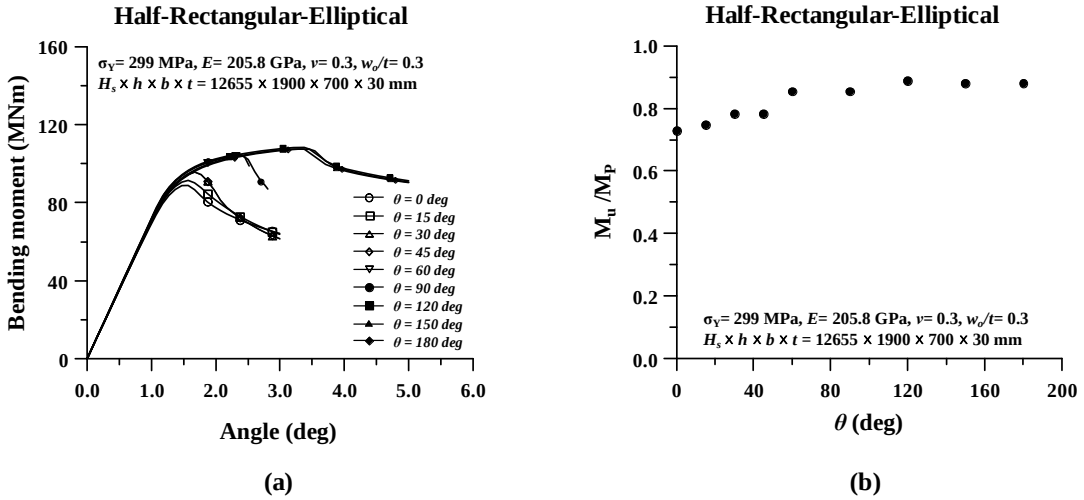

Fig. 19. Effect of cutout's angle under pure bending: (a) moment-rotation histories; (b) non-dimensionalized load carrying strength.

Fig. 18 illustrates an example of applied geometries varying cutout's angle in circumferential direction, $\theta = 0$~180 degree. Fig. 19 represents moment-rotation histories varying cutout's angle and the non-dimensionalized load carrying strength. It is confirmed that when the cutout locates on compression side ($\theta = 0$ degree), the ultimate strength shows the minimum strength and as the cutout's angle increases, so does the ultimate strength. It is observed that the ultimate strength increases almost linearly until $\theta = 90$ degree whereas it appears almost constant over 90 degrees ($\theta = 120$, 150, 180 degree).

5.2.3. Combined effects of aspect ratio, column slenderness ratio and column aspect ratio

To examine the effects of aspect ratio, column slenderness ratio and column aspect ratio on the ultimate strength, the dimensions of the cutout varies from the boundaries of statistical distribution, $1800 \leq h \leq 2900$, $600 \leq b \leq 1100$, as illustrated in Section 3.2. For the selection of parameters, DOE by using CCD method is applied. Four cases of the maximum diameter varying from 2750 mm to 4250 mm are taken into account with the locations of the cutout in vertical- and circumferential-direction, $h_o / H_S = 0.1$ and $\theta = 0$ degree. Thousand eighty cases of series analyses are performed in total. The parameters considered in this section are as follows:

- Shape: rectangular, elliptical, half-rectangular-elliptical
- Height of the cutout, h : 1800~2900 mm
- Width of the cutout, b : 600~1100 mm
- Column slenderness ratio, $\lambda = D_{\max} / t$: 90, 110, 125, 130, 150
- Diameter, $D_{\max}$: 2750, 3250, 3750, 4250 mm
- Loading condition: axial compression and pure bending

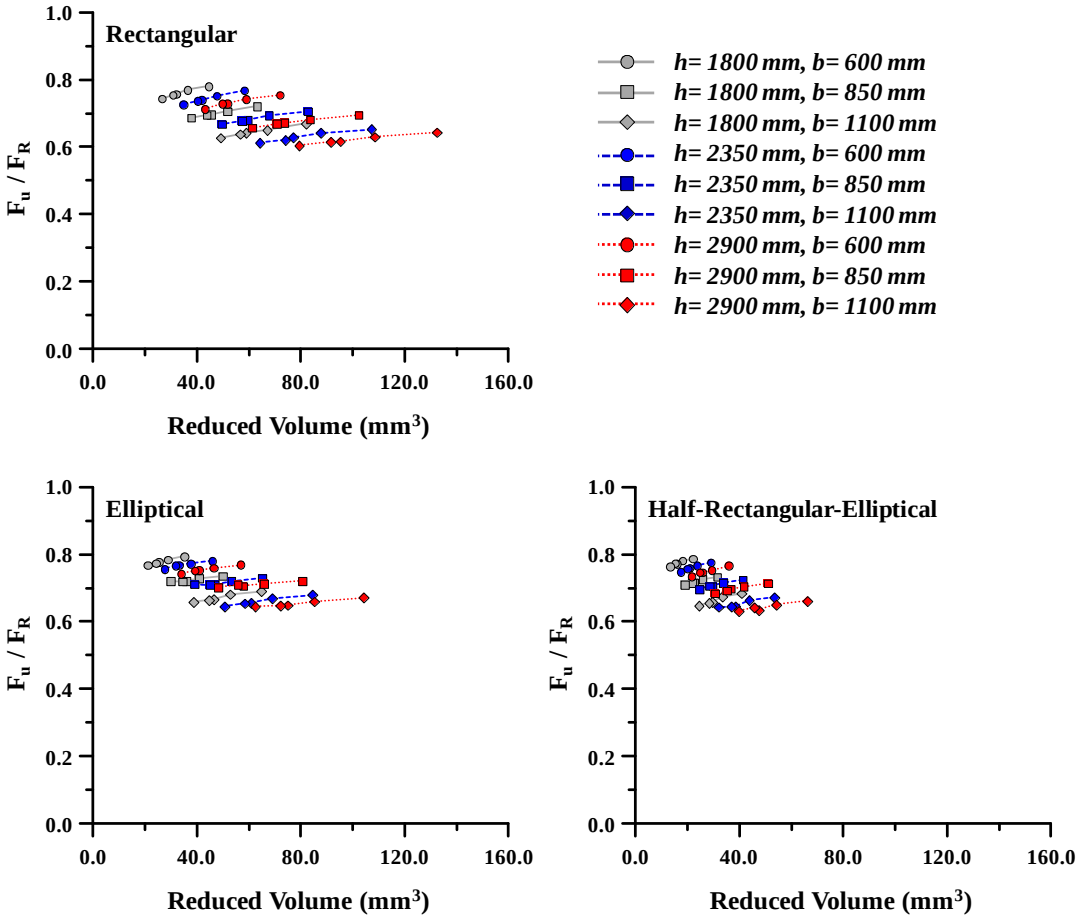

Fig. 20. An example of effect of column slenderness ratio for $D_{\max} = 3750$ mm under axial compression.

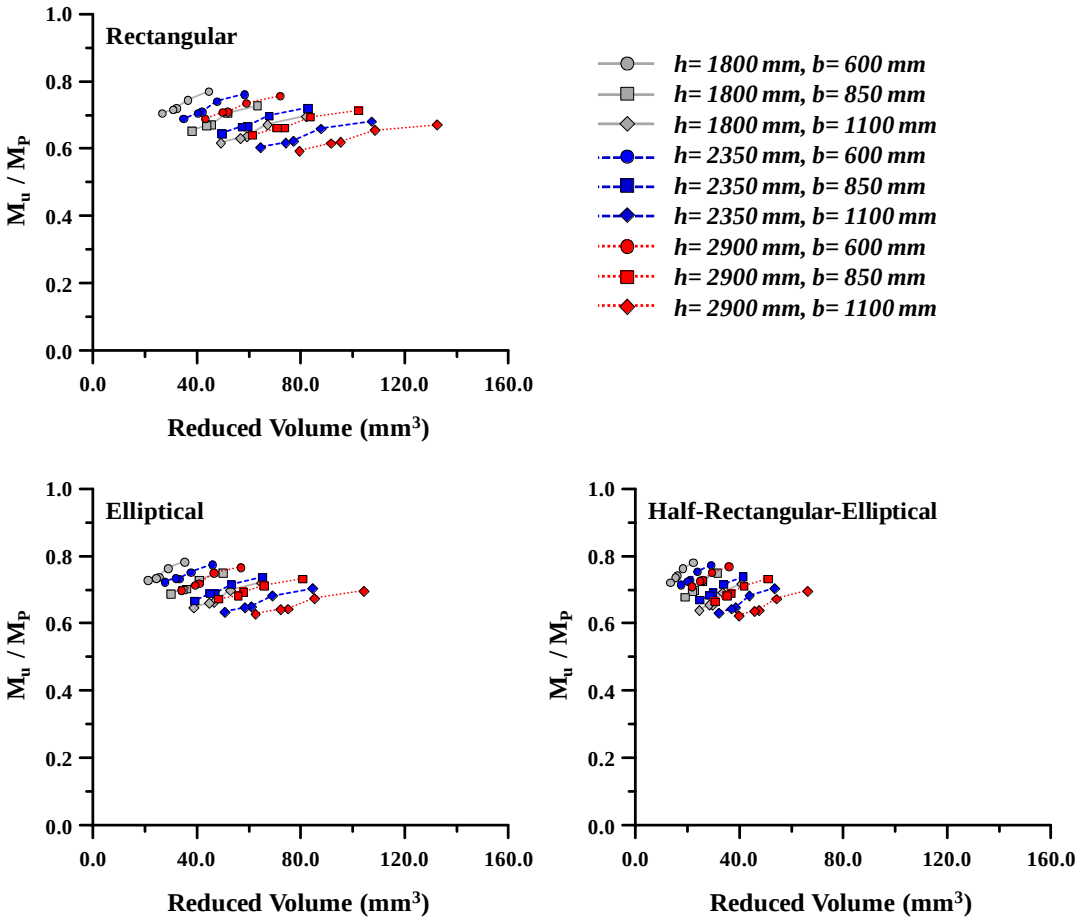

Fig. 21. An example of effect of column slenderness ratio for $D_{\max}$ = 3750 mm under pure bending.

Table A2 in Appendix summarizes the selected design points by using CCD. Figs. 20 and 21 show an example of the effect of column slenderness ratio on the non-dimensionalized ultimate strength ($D_{\max}$ = 3750 mm) for three shapes under axial compression and pure bending. It has been observed that as the reduced volume increases, it lowers the strength and the reduced strength appears nearly the same regardless of the shape. Figs. 22 and 23 illustrate the non-dimensionalized ultimate strength of selected design points for 3-shape of cutouts under axial compression and pure bending. It is found that the ultimate strength reduction appears within the range from 50% to 80% of reference strength for both loading conditions.

6. Empirical Formulation of the Ultimate Strength

The results of the parametric analysis described in Section 5.3 are used to derive empirical formulations of predicting the ultimate strength of the circular cylindrical shell with the cutout. Linear regression equations with least square method are used, as follows:

$$F_u / F_R = \xi_D D_{\max} + \xi_t t + \xi_h h + \xi_b b + \xi_C \quad (3)$$

$$M_u / M_P = \zeta_D D_{\max} + \zeta_t t + \zeta_h h + \zeta_b b + \zeta_C \quad (4)$$

In the above, F_u / F_R and M_u / M_P are the non-dimensionalised ultimate strength of axial compression and pure bending, respectively.

The coefficients of the design formula for axial compression and pure bending are indicated in Table 3. Regression statistics including the correlation coefficients and the adjusted R-square are illustrated in Table 4. A correlation between numerical results and the empirical estimations on the

ultimate strength of circular cylindrical shells with the cutout is illustrated in Fig. 24. It is found that the estimations by the proposed empirical equations well agree to the numerical calculations. This implies that the proposed empirical equations can be an effective measure of estimating the reduced ultimate strength of circular cylindrical shells with the cutout.

While the design formulae developed in the present study cover an extensive range of possible geometrical variations in circular cylindrical shells with the cutout and they must be a good guidance for wind turbine tower design. It should be cautioned that they may need to be validated further by comparison with more specific computations and experiments when one may aim at using them for some special cases of geometric and boundary conditions.

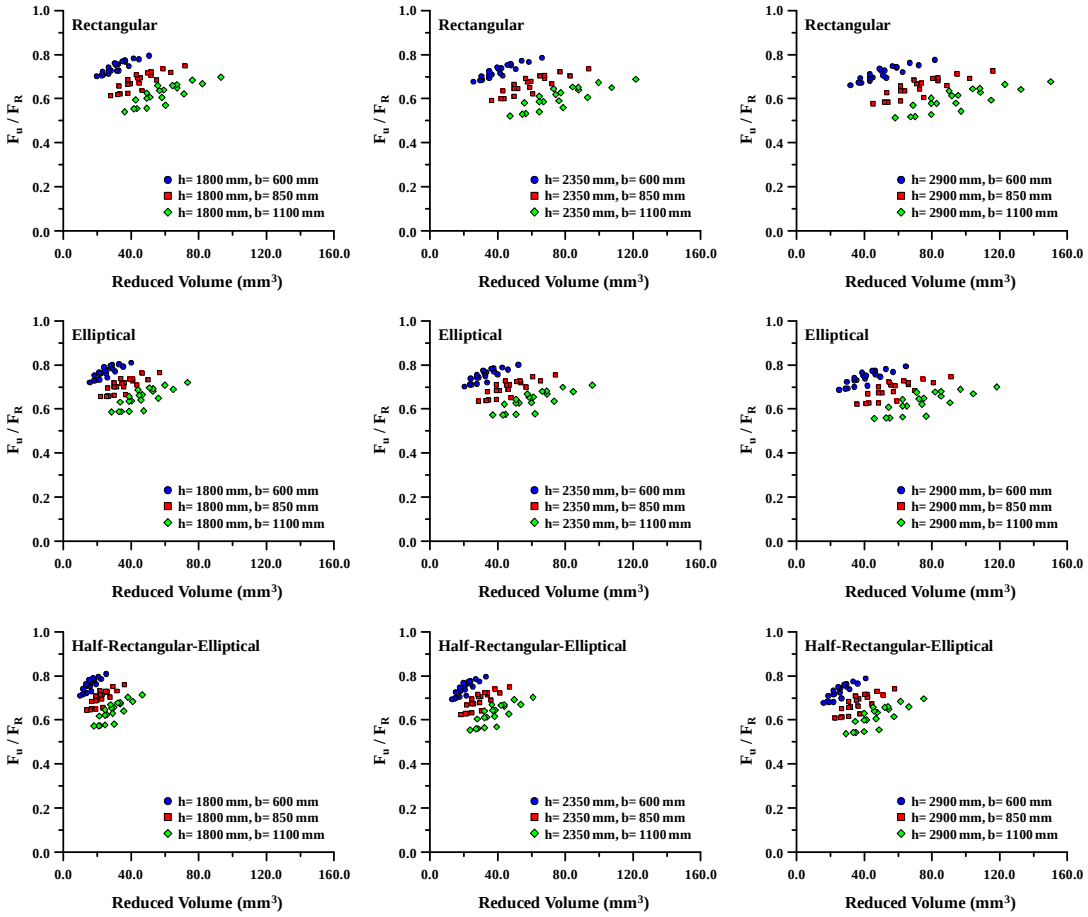

Fig. 22. Summary of the non-dimensionalized ultimate strength under axial compression.

Table 3. Coefficients of design formula

Shape	Axial Compression				
	ξ_D (10^{-6})	ξ_t (10^{-3})	ξ_h (10^{-6})	ξ_b (10^{-3})	ξ_C
Rectangular	0.486	2.206	-0.248	-0.245	0.698
Elliptical	0.505	1.407	-0.214	-0.229	0.723
Half-Rectangular-Elliptical	0.512	1.700	-0.239	-0.235	0.713
Shape	Pure Bending				
	ζ_D (10^{-6})	ζ_t (10^{-3})	ζ_h (10^{-6})	ζ_b (10^{-3})	ζ_C
Rectangular	-0.141	4.250	-0.151	-0.187	0.791
Elliptical	-0.144	3.661	-0.175	-0.172	0.827
Half-Rectangular-Elliptical	-0.148	3.984	-0.175	-0.176	0.818

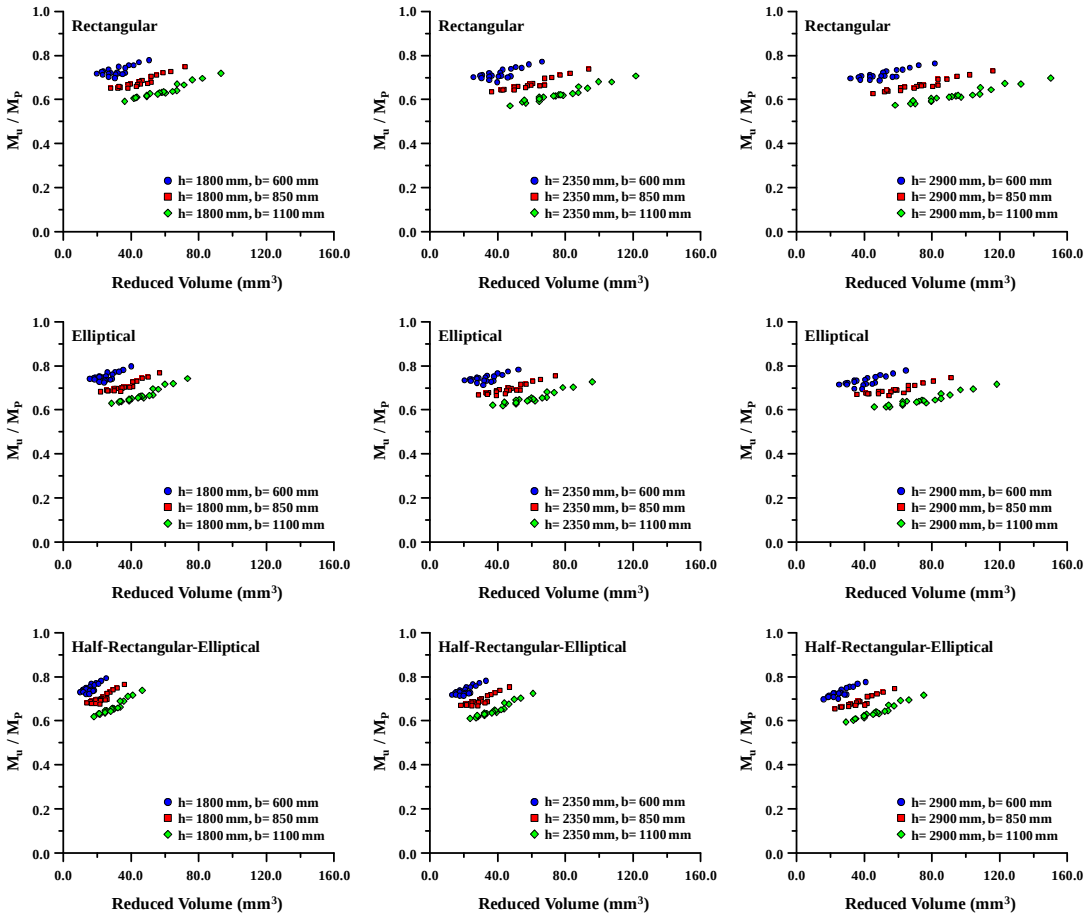

Fig. 23. Summary of the non-dimensionalized ultimate strength under pure bending

7. Conclusion

The aims of this study are to develop numerical modelling technique accurately predicting structural response taking into account nonlinearities and to numerically examine the effects of various variables on the ultimate-strength characteristics of wind turbine towers with the cutout. A series of nonlinear finite element computations are undertaken to achieve these objectives. Several conclusions can be drawn from the results, as outlined below.

- First, the wind turbine structures in service are investigated. The actual dimensional characteristics of these wind turbine structures and cutouts are identified from the data collected and analyzed.
- The nonlinear finite element modelling technique is developed based the mesh convergence study and validation studies for wind turbine towers with the cutout.
- It is confirmed that the effect of cutout's shape is negligible and the cutout's location on compression side shows the minimum ultimate strength. Further, under pure bending, the ultimate strength appears in uniform when the cutout angle is over 90 degree.

Table 4. Regression statistics

Shape	Axial Compression		Pure Bending	
	σ	R^2	σ	R^2
Rectangular	0.989	0.977	0.975	0.950
Elliptical	0.989	0.977	0.972	0.943
Half-Rectangular-Elliptical	0.989	0.978	0.978	0.956

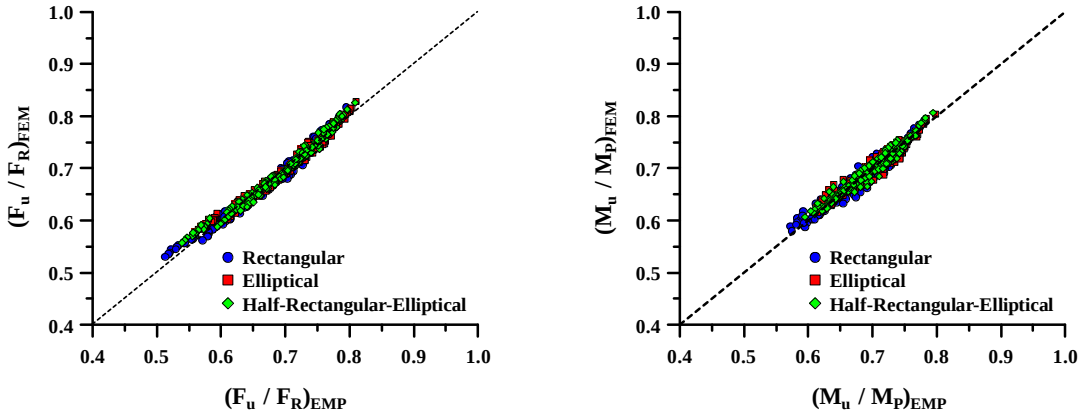

Fig. 24. Correlation between the FEA and empirical estimation on the ultimate strength.

- Based on the results of the parametric analysis, a design formula accommodating a whole range of actual dimensional characteristics is proposed. This formula has the potential to improve the design and safety assessment of circular cylindrical shells with the cutout.
- Considering that a lots of uncertainties are involved due to geometrical and boundary conditions, among others, further researches are recommended to conduct experiments on models which will be used to examine the collapse mechanism more realistically.

Acknowledgements

This research was supported by Basic Science Research Program through the National Research Foundation of Korea (NRF) funded by the Ministry of Education (NRF-2014R1A1A2006102 and NRF-2015R1A6A3A01060166). Also, this study was undertaken at The Lloyd's Register Foundation Research Centre of Excellence at Pusan National University. Lloyd’s Register Foundation (LRF), a UK registered charity and sole shareholder of Lloyd’s Register Group Ltd, invests in science, engineering and technology for public benefit, worldwide.

Appendix A.

A.1. Tables

Table A1. Principal dimensions of wind turbines and cutouts

No.	Capacity (MW)	H (mm)	D_{Min} (mm)	D_{Max} (mm)	T_{Min} (mm)	T_{Max} (mm)	h (mm)	b (mm)	t (mm)
1	1.0	45	2090	3280	10	18	2000	700	18
2	2.0	50	2560	4150	16	36	2550	850	36
3	2.0	53	2580	4040	18	36	2550	850	36
4	3.0	65	2280	4150	14	28	2550	850	28
5	3.0	60	2350	4052	16	32	2550	850	32
6	5.0	75	2450	6000	16	27	2550	850	27
7	5.0	75	2570	6000	16	27	2550	850	27
8	0.45	37	1820	2800	10	16	2050	700	16
9	0.6	40	1800	2720	10	18	2180	720	18
10	2.0	60	2300	3750	18	30	2690	1100	30
11	3.0	100	2540	4500	18	30	2150	703	30
12	4.0	92	2460	4300	14	30	2540	990	30
13	3.5	88	2320	4150	16	34	1640	750	34
14	2.0	76	3000	4300	12	30	2150	850	30
15	3.7	77	3000	4000	15	40	2900	850	40

No.	Capacity (MW)	H (mm)	D_{Min} (mm)	D_{Max} (mm)	T_{Min} (mm)	T_{Max} (mm)	h (mm)	b (mm)	t (mm)
16	2.0	50	2850	4150	20	40	2900	850	40
17	3.0	65	2294	3650	14	28	1997	750	28
18	3.2	60	2150	3720	16	32	2080	800	32
19	2.0	48	2000	3570	18	34	1850	680	34
20	4.2	88	2380	4420	14	34	2200	850	34
21	2.6	70	2210	2980	16	28	1920	700	28
22	2.2	65	2370	3020	16	28	1900	680	28
23	2.7	69	2450	2950	14	30	2100	680	30
24	3.4	70	2340	3800	16	30	2020	750	30
25	4.2	80	2240	3650	14	32	1980	680	32
26	2.0	55	2200	3400	14	28	1900	720	28
27	2.9	85	2320	3860	14	30	2080	780	30
28	2.9	75	2460	3680	14	28	2280	820	28
29	1.8	50	1780	2900	16	28	1870	690	28
30	3.7	78	2240	3780	14	32	1990	750	32
31	3.0	70	2370	3720	14	28	1930	680	28
32	1.8	55	1890	2890	16	28	1880	680	28
33	2.2	60	1920	3220	14	30	2050	720	30
34	3.4	78	2360	3680	14	30	1990	680	30
35	3.2	65	2280	3540	16	28	1920	800	28
36	2.6	55	2360	3640	14	26	1900	680	26
37	1.8	50	1760	2700	14	28	1840	680	28
38	1.7	55	1680	2740	12	26	1900	650	26
39	3.5	68	2320	3640	14	30	1960	700	30
40	2.7	65	2240	3580	14	32	1990	780	32
41	3.4	84	2450	3840	16	28	2000	800	28
42	3.0	65	2280	3480	16	30	1980	720	30
43	1.6	50	1780	2690	14	28	1780	780	28
44	2.6	60	1880	3640	16	30	1990	680	30
45	3.0	70	2264	3700	12	32	2040	720	32
46	3.6	68	2380	3680	14	32	1980	640	32
47	2.3	50	2210	3200	12	28	1880	684	28
48	1.8	50	1760	2700	14	28	1840	680	28
49	1.6	55	1720	2860	12	28	1880	650	28
50	3.6	73	2260	3680	14	32	1994	686	32
51	2.4	55	2200	3400	14	28	1800	640	28
52	4.1	78	2260	4100	14	32	2100	780	32
53	1.8	52	2140	3360	12	22	1980	720	22
54	2.6	65	2420	3860	16	32	2860	780	32
55	2.4	60	2380	3900	16	34	2200	650	34
56	2.0	55	1980	3450	12	30	2640	700	30
57	3.4	65	2340	3640	14	34	1980	660	34
58	1.9	50	1840	2640	14	26	2000	700	26
59	5.0	88	2570	4230	16	32	2240	650	32
60	0.8	40	1750	2900	10	28	1990	650	28
61	4.0	80	1900	2890	14	28	2000	720	28
62	2.0	64	2320	3840	14	30	2720	980	30
63	3.2	80	2640	3840	14	32	2080	680	32

No.	Capacity (MW)	H (mm)	D_{Min} (mm)	D_{Max} (mm)	T_{Min} (mm)	T_{Max} (mm)	h (mm)	b (mm)	t (mm)
64	4.0	75	2360	4180	14	28	2120	640	28
65	3.1	65	2240	3680	16	32	1970	680	32
66	4.0	80	2320	3860	12	28	1990	690	28
67	3.4	83	2360	3940	12	32	2220	710	32
68	2.4	60	2240	2940	10	28	1940	650	28
69	1.8	50	1780	2680	12	24	1890	640	24
70	2.1	74	2400	3620	10	32	2100	680	32
71	3.4	78	2180	3680	12	34	2200	740	34
72	2.2	52	1860	2870	10	28	2050	650	28
73	2.8	68	2150	3720	12	32	1940	680	32
74	3.4	68	2240	3640	14	28	2000	660	28
75	2.2	55	1990	2870	16	30	1980	720	30
76	3.9	84	2280	3640	14	28	2120	750	28
77	2.6	80	2180	3640	12	30	1990	680	30
78	2.4	60	2120	3360	12	32	1970	710	32
79	2.6	67	2240	3420	12	26	1990	672	26
80	3.1	80	2180	3640	14	32	1940	690	32
81	3.0	72	2140	3480	12	32	2130	700	32
82	2.1	65	1960	3580	12	32	1980	640	32
83	3.3	80	2240	4000	12	32	2200	840	32
84	2.4	64	2260	3800	14	32	2120	680	32
85	1.7	52	1790	3140	12	32	1980	720	32
86	3.7	78	2240	3780	14	32	1990	750	32
87	2.8	72	2260	3450	12	30	2050	750	30
88	1.9	55	1680	3120	12	30	1960	724	30
89	2.4	68	1890	3480	13	28	2150	750	28
90	3.7	87	2480	3780	12	32	2040	750	32
91	3.4	80	2340	3750	14	32	2000	810	32
92	2.7	68	2180	3580	12	30	2000	780	30
93	2.1	64	1860	2940	10	28	1960	680	28
94	2.0	60	1600	2900	16	30	1880	750	30
95	3.2	66	2200	3690	10	28	1890	690	28
96	2.4	60	2140	3640	10	30	1800	640	30
97	3.0	80	2200	3450	12	30	1920	740	30
98	2.4	72	2180	3590	14	32	2100	720	32
99	1.4	45	1640	2610	10	26	1680	620	26
100	3.1	65	1960	3580	12	28	1890	690	28
101	2.7	65	2230	3690	14	28	2200	740	28
102	3.4	73	2240	3640	12	27	2050	700	27

Table A2. An example of selected design points by DOE with CCD method

No.	D/t	h (mm)	b (mm)	No.	D/t	h (mm)	b (mm)
DP1	90			DP26	90		
DP2	110			DP27	110		
DP3	125	1800	600	DP28	125	2900	1100
DP4	130			DP29	130		
DP5	150			DP30	150		
DP6	90			DP31	90		
DP7	110			DP32	110		
DP8	125	1800	850	DP33	125	2900	600
DP9	130			DP34	130		
DP10	150			DP35	150		
DP11	90			DP36	90		
DP12	110			DP37	110		
DP13	125	1800	1100	DP38	125	2900	850
DP14	130			DP39	130		
DP15	150			DP40	150		
DP16	90			DP41	90		
DP17	110			DP42	110		
DP18	125	2350	600	DP43	125	2900	1100
DP19	130			DP44	130		
DP20	150			DP45	150		
DP21	90						
DP22	110						
DP23	125	2350	850	-			
DP24	130						
DP25	150						

References

ANSYS, 2015. User's manual (version 16.1). ANSYS Inc., Canonsburg, PA, USA.

Azizian ZG and Roberts TM. 1983. Buckling and elasto-plastic collapse of perforated plates. Proceedings of the International Conference on Instability and Plastic Collapse of Steel Structures, Granada Publishing, London, UK, pp. 392-398.

Betten J and Shin CH. 2000. Elasto-plastic buckling analysis of rectangular plates subjected to biaxial loads. Forschung im Ingenieurwesen, 65: 273-278.

Brazier LG. 1927. On the flexure of thin cylindrical shells and other "thin" sections. Proceedings of Royal Society of London, Series A. 116(773): 104–114.

Brown CJ and Yettram AL. 1986. The elastic stability of square perforated plates under combinations of bending, shear and direct load. *Thin-Walled Structures*, 4(3): 239-246.

Collu M, Brennan FP and Patel MH. 2014. Conceptual design of floating support structure for an offshore vertical axis wind turbine: the lessons learnt. *Ships and Offshore Structures*, 9(1): 3-21.

Dimopoulos CA and Gantes CJ. 2012. Experimental investigation of buckling of wind turbine tower cylindrical shells with opening and stiffening under bending. *Thin-Walled Structures*, 54: 140-155.

DIN 18800-4. 1990. Stahlbauten: Stabilitätsfälle, Schalenbeulen, Beuth Verlag, Berlin, Germany.

DNVGL. 2013a. Design of offshore wind turbine structures. Report No.: DNV-OS-J101, Det Norske Veritas, Oslo, Norway.

DNVGL. 2013b. Buckling strength of shells. DNV-RP-C202, Det Norske Veritas, Oslo, Norway.

Durban D and Zuckerman Z. 1999. Elasto-plastic buckling of rectangular plates in biaxial compression/tension. *Int. Journal of Mechanical Science*, 41: 751-765.

ECCS. 1980. Technical Committee 8, Structural Stability, TWG 8.4-Shells, Buckling of Steel Shells. European Design Recommendations, 1st edition.

El-Sawy KM, Nazmy AS and Martini MI. 2004. Elasto-plastic buckling of perforated plates under uniaxial compression. *Thin-Walled Structures*, 42: 1083-1101.

EN1993-1.6. 2006. European Committee for Standardization, Eurocode 3: Design of Steel Structures, Part 1–6: Strength and Stability of Shell Structures.

EWEA. 2014. Wind in power, 2014 European statistics, European Wind Energy Association, Brussels, Belgium, Available online: http://www.ewea.org/fileadmin/files/library/publications/statistics /EWEA- Annual-Statistics-2014.pdf.

Fabian O. 1977. Collapse of cylindrical, elastic tubes under combined bending, pressure and axial loads. *Int. Journal of Solids Structures*, 13: 1257-1270.

Gellin S. 1980. The plastic buckling of long cylindrical shell under pure bending. *Int. Journal of Solids Structures*, 16: 397-407.

Ghazijahani TG, Jiao H and Holloway D. 2015. Structural behaviour of shells with different cutouts under compression: An experimental study. *Journal of Construction Steel Research*, 105: 129-137.

Guo L, Yang S and Jiao H. 2013. Behaviour of thin-walled circular hollow section tubes subjected to bending. *Thin-Walled Structures*, 73: 281-289.

Han H, Cheng J, Taheri F and Pegg N. 2006. Numerical and experimental investigations of the response of aluminum cylinders with a cutout subject to axial compression. *Thin-Walled Structure*, 44: 254-270.

Jensen FM, Falzon BG, Ankersen J and Stang H. 2006. Structural testing and numerical simulation of 34m composite wind turbine blade. *Composite Structures*, 76: 52-61.

Ju GT and Kyriakides S. 1992. Bifurcation and localization instabilities in cylindrical shells under bending II. Predictions. *Int. Journal of Solids Structures*, 29: 1143-1171.

Jullien J and Limam A. 1998. Effects of openings of the buckling of cylindrical shells subjected to axial compression. *Thin-Walled Structure*, 31: 187-202.

Kim UN, Choe IH and Paik JK. 2009. Buckling and ultimate strength of perforated plate panels subject to axial compression: experimental and numerical investigations with design formulations. *Ships and Offshore Structures*, 4(4): 337-361.

Kyriakides S and Ju GT. 1992. Bifurcation and localization instabilities in cylindrical shells under bending. I. Experiments. *Int. Journal of Solids Structures*, 29: 1117-1142.

Kühlmeier L. 2007. Buckling of wind turbine rotor blades. Analysis, design and experimental validation, PhD thesis, Aalborg University, Denmark, ISBN: 87-91464-00-5.

Lee HG and Park J. 2016. Static test until structural collapse after fatigue testing of a full-scale wind turbine blade. *Composite Structures*, 136: 251-257.

Overgaard LCT, Lund E and Camanho PP. 2010a. A methodology for the structural analysis of composite wind turbine blades under geometric and material induced instabilities. *Composite Structures*, 88: 1092-1109.

Overgaard LCT, Lund E and Thomsen OT. 2010b. Structural collapse of a wind turbine blade, Part A: static test and equivalent single layered models. Composites Part A: Applied Science and Manufacturing, 41: 257-270.

Overgaard LCT and Lund E. 2010. Structural collapse of a wind turbine blade, Part B: progressive interlaminar failure models, Composites Part A: Applied Science and Manufacturing, 41: 271-283.

Paik JK. 2007. Ultimate strength of steel plates with a single circular hole under axial compressive loading along short edges. *Ships and Offshore Structures*, 2(4): 355-360.

Reissner E. 1961. On finite pure bending of cylindrical tubes. *Ö sterreichisches Ingenieur-Archiv*, 15: 165-172.

Sabir AB and Chow FY. 1983. Elastic buckling of flat panels containing circular and square holes. Proceedings of the International Conference on Instability and Plastic Collapse of Steel Structures, Granada Publishing, London, UK, pp. 311-321.

Schenk CA and Schuëller GI. 2007. Buckling analysis of cylindrical shells with cutouts including random boundary and geometric imperfections. *Cimputer Methods in Applied Mechanics and Engineering*, 196: 3424-3434.

Seide P and Weingarten VI. 1961. On the buckling of circular cylindrical shells under pure bending. *Journal of Applied Mechanics*, 28: 112-116.

Shangmugam NE, Thevendran V and Tan YH. 1999. Design formula for axially compressed perforated plates. *Thin-Walled Structures*, 34(1): 1-20.

Shariati M and Rokhi MM. 2008. Numerical and experimental investigations on buckling of steel cylindrical shells with elliptical cutout subject to axial compression. *Thin-Walled Structure*, 46: 1251-1261.

Shariati M and Rokhi MM. 2010. Buckling of steel cylindrical shells with an elliptical cutout. *Int. Journal of Steel Structures*, 10: 193-205.

Sherman DR. 1976. Tests of circular steel tubes in bending. *ASCE Journal of the Structural Division*, 102: 2181-2195.

Tennyson RC. 1968. The effects of unreinforced circular cutouts on the buckling of circular cylindrical shells under axial compression. *Journal of Engineering for Industry*, 90(4): 541-546.

Wang G, Sun H, Peng H and Uemori R. 2009. Buckling and ultimate strength of plates with openings. *Ships and Offshore Structures*, 4(1): 43-53.

Yang J, Peng C, Xiao J, Zeng J, Xing S and Jin J. 2013. Structural investigation of composite wind turbine blade considering structural collapse in full-scale static tests. *Composite Structures*, 97: 15–29.

Yeh MK, Lin MC, and Wu WT. 1999. Bending Buckling of an Elasto-plastic Cylindrical Shell with a Cutout. *Engineering Structures*, 21: 996-1005.